Powder Technology 354 (2019) 765–778

Contents lists available at ScienceDirect

Powder Technology

journal homepage: www.elsevier.com/locate/powtec

On the dynamics and control of continuous fluidized bed layering granulation with screen-mill-cycle

C. Neugebauer [a], E. Diez [b], A. Bück [c], S. Palis [a], S. Heinrich [b], A. Kienle [a,d,*]

[a] Automation / Modeling, Otto von Guericke University, Magdeburg, Germany
[b] Institute of Solids Process Engineering and Particle Technology, Hamburg University of Technology, Hamburg, Germany
[c] Institute of Particle Technology, Friedrich-Alexander University Erlangen-Nürnberg, Erlangen, Germany
[d] Max Planck Institute for Dynamics of Complex Technical Systems, Magdeburg, Germany

ARTICLE INFO

Article history:
Received 22 March 2019
Received in revised form 7 May 2019
Accepted 11 May 2019
Available online 22 May 2019

Keywords:
Fluidized bed layering
Continuous operation
Stability
Control

ABSTRACT

This paper is concerned with an experimental and theoretical study of dynamics and control of fluidized bed layering granulation with external screen mill cycle. To achieve quantitative agreement between model calculations and experiments an extended dynamic process model is proposed. In contrast to previous work by Dreyschultze et al. [1] specific plant characteristics are taken explicitly into account including a more detailed model of the milling process and a classifying particle withdrawal from the granulation chamber. The model is then used to develop new control strategies. First, a novel bed mass controller is designed and validated. Afterward, a second control loop is introduced to dampen the oscillatory behavior of the particle size distribution. It is shown that the new control concepts achieve stable steady-state operation within a short time and thereby improve the process dynamics significantly. Theoretical predictions and experimental results are shown to be in good agreement.

1. Introduction

In fluidized bed layering granulation (FBLG), product granules of high quality are formulated by spraying a solid-containing liquid, e.g. a solution or suspension, onto a bed of particles fluidized with a heated gas [2]. While the liquid fraction of the injection evaporates, the solid fraction remains on the surface of the particles inducing a layer-wise growth [3]. For high production rates, FBLG is operated as a continuous process. Since product particles are continuously removed, this in turn requires a continuous supply of new nuclei. This can be achieved either by internal nucleation due to thermal overspray [4] or grinding of oversized particles [5].

As was shown by means of experiments, presented by Schütte et al. [6] and Schmidt et al. [7–9], continuous FBLG tends to instabilities in the form of self-sustained non-linear oscillations of the particle size distribution (PSD). These oscillations lead to variations in the product properties or, in the worst case, may even lead to a breakdown of the granulation process. They are therefore highly undesired. To clarify the potential reasons for these instabilities, different processes configurations were studied by means of model-based analysis. While the authors Vreman et al. [10] and Neugebauer et al. [11] studied the dynamics of FBLG with internal nucleation, Radichkov et al. [12] and Dreyschultze et al. [1] put the focus on FBLG with formation of seed particles by milling of oversized particles. All contributions revealed a significant impact of the operating conditions on the dynamic stability. However, besides stability, the operating parameters also affect the particle properties: The contributions of Hoffmann et al. [13], Rieck et al. [14], and Diez et al. [15] proved the dependency of selected particle characteristics, for instance, particle porosity, on the thermal conditions inside the granulation chamber. Therefore, a careful selection of operating parameters is essential for the formation of particles with tailor-made properties under stable conditions. In addition, it has been shown theoretically that the application of feedback control strategies is promising to enhance the dynamic stability and the transient behavior of continuous FBLG. Palis & Kienle [16] showed that a linear PI-controller is capable to stabilize continuous FBLG processes in the neighborhood of some given reference point. The robustness can be increased by H_∞ loop shaping as presented by Palis & Kienle [16,17]. Further suitable approaches to enhance process stability and the dynamics are adaptive control strategies [18,19], model predictive control [20,21], and non-linear control strategies as discrepancy based control [22,23]. In multi-stage operation the process chamber is subdivided into compartments with different functionalities leading to additional measurements and actuating values. Therefore, Cotabarren et al. [24] and Palis [25] introduced multiple input multiple output control strategies for this type of processes. Even though the simulation results of the

* Corresponding author.
E-mail address: kienle@mpi-magdeburg.mpg.de (A. Kienle).

https://doi.org/10.1016/j.powtec.2019.05.030

different control approaches are quite promising, an experimental implementation and validation is still missing.

This gap is closed in the present paper. Focus is on continuous FBLG with screen-mill-cycle as presented in Fig. 1: Particles are withdrawn from the granulation chamber via a rotary valve and classified by screening into fine, product and oversized fraction. After milling, the oversized fraction is, together with the fines, re-fed to the granulation chamber while product particles are removed from the process. The experiments are carried out in a pilot plant located at TU Hamburg. Besides control of PSD, special attention is also given to the control of the bed mass, which turned out to be non-trivial and is a necessary prerequisite for stable long term operation of the plant. Furthermore, an extended mathematical model of the plant is presented and compared to the experimental findings.

The remainder of the present paper is structured as followed: In the upcoming Section 1.1 a detailed process description is given. The dynamic model of the investigated FBLG is introduced in Section 2. The results of the experiments are presented and compared to simulation results in the subsequent Section 3. First, focus is on bed mass control. Afterward, control of PSD is addressed. Using the developed mathematical model a corresponding controller is designed to dampen the particle size distribution. Finally, the results of this contribution are summarized and an outlook on future directions is presented in Section 4.

1.1. Process description

The experimental examination has been carried out in a horizontal fluidized bed plant of type *Procell 25* of the manufacturer *Glatt GmbH*, Weimar, Germany. The process chamber, presented in Fig. 2, has a width of 1.00 m, a depth of 0.25 m and a height of 0.40 m and can be divided into four different compartments by introducing weirs. However, throughout this contribution, no weirs were used and the granulator was operated as a single process chamber with uniform conditions due to intensive mixing. All presented experiments were performed under similar conditions. At the start of each experiment, sodium benzoate particles of the overall mass of 27.5 kg were fed to the process chamber. The particles were fluidized by fluidization medium. For this purpose, ambient air was heated up to 85 °C and blown into the granulation chamber. A proper choice of the fluidization conditions is crucial for the FBLG. Too little fluidization air induces a too small fluidization velocity u_{fluid} resulting in an insufficient fluidization of the particles. Otherwise, too much fluidization air leads to the blow out of the bed since u_{fluid} is too high. An overview of the fluidization conditions, based on [2], is presented in Fig. 3. There, the minimum fluidization velocity is denoted as u_{mf} while u_{elu} describes the permissible maximum value of u_{fluid}. Throughout the experimental investigations, the fluidization velocity u_{fluid} is 2.3 m/s.

The injected solution consists of 35 wt% sodium benzoate dissolved in demineralized water. Per hour of process time 40 kg solution were atomized by three two-fluid nozzles located at the bottom of the granulation chamber. As atomizing gas compressed air was used. The injected droplets sprinkled the particles surface. Due to the enhanced heat exchange between particles and fluidization medium, the liquid phase of the droplets evaporated. The vapor was carried out by the fluidization medium. Because of the evaporation, the temperature of the fluidization medium within the process chamber decreased to 50 °C. Meanwhile, the remaining sodium benzoate solidified on the particles surface inducing the layering-growth. Under the examined process conditions, layering was the dominant granulation mechanism. In accordance with Ennis et al. [26], the influence of agglomeration, attrition, and internal nucleation, was limited by an appropriate choice of the operating parameters.

Particles were withdrawn from the granulation chamber by a rotary valve. The utilized valve is shown in Fig. 2. The discharged particles were transported to a two-deck tumbler screen by pneumatic conveyance. According to the mesh width of the screens, the particles were classified into three fractions: The fines fraction consists of particles smaller than 0.8 mm, the product fraction comprises particles in the range of 0.8 mm to 1.2 mm, and the oversized fraction contains particles larger than 1.2 mm. While the product fraction was removed from the process, the oversized fraction was milled and, together with the fines fraction, re-fed to the granulation chamber. For grinding of the oversized particles an impact mill of type *Rekord A* of *Gebr. Jehmlich GmbH, Nossen, Germany* was utilized. As illustrated in Fig. 2, the mill was equipped with pin-mill grinding elements.

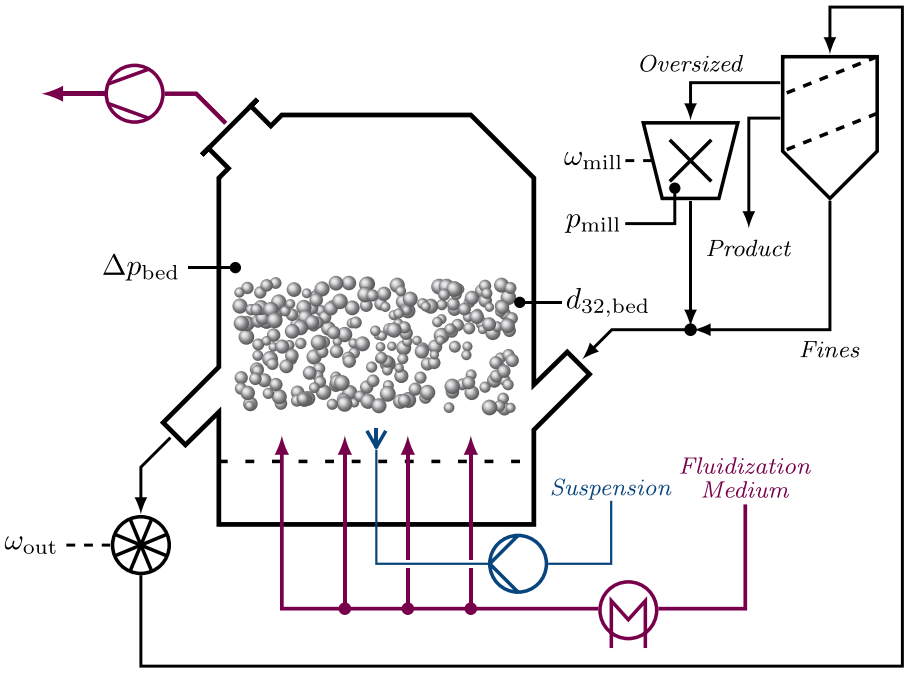

Fig. 1. Process scheme of fluidized bed layering granulation (FBLG) with external screen-mill-cycle.

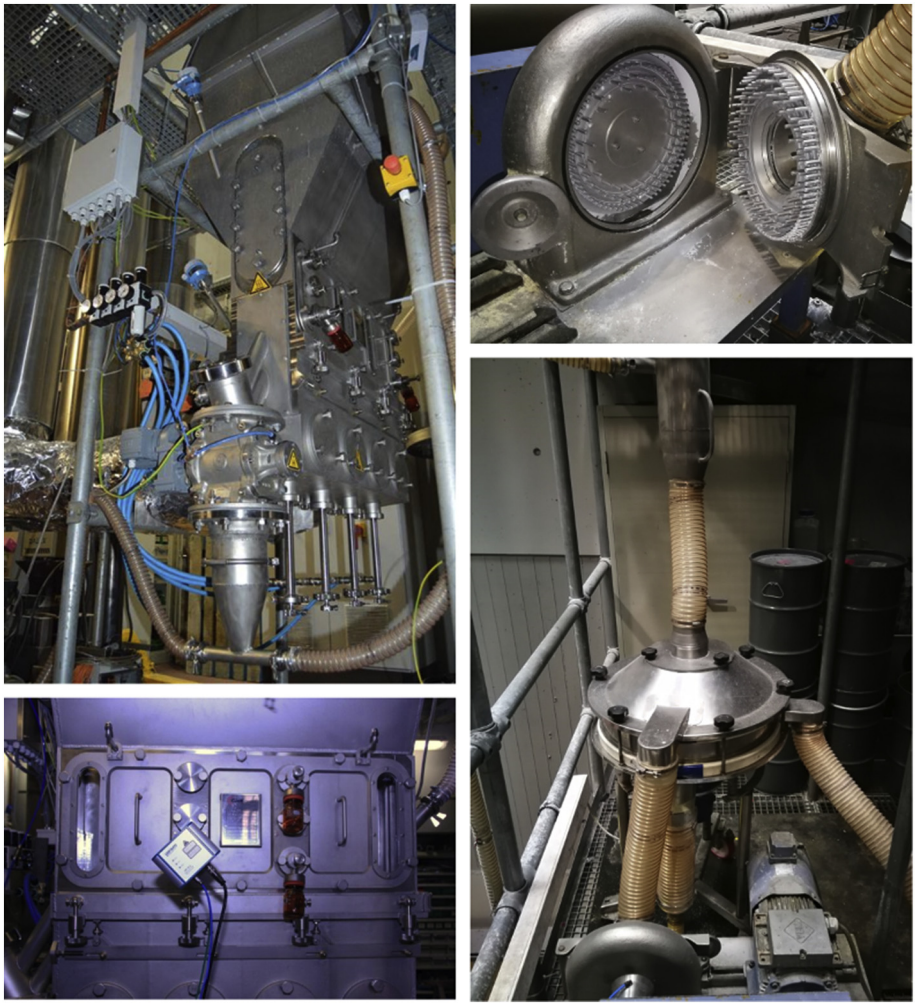

Fig. 2. Pictures of the utilized equipment: **Upper Left:** Granulation chamber *Procell 25* of Glatt GmbH. **Lower Left:** Granulation chamber equipped with Parsum Probe and sampling device. **Upper Right:** Impact mill equipped with pin-mill grinding elements. **Lower Right:** Two-deck-tumbler screen and impact mill.

To obtain online information about the particle sizes, the process chamber was equipped with the inline probe *IPP 70-S (Parsum GmbH, Chemnitz, Germany)*. Based on spatial filter velocimetry (Petrak [27]), the probe determines the chord length distribution of the measured particles, which was used for control purposes. In addition, particle samples of the bed and the outlet were taken every 20 minutes. By means of digital imaging processing, the particle size distributions of those samples were determined with a CamSizer XT (Retsch Technology GmbH, Haan, Germany) in the post-processing.

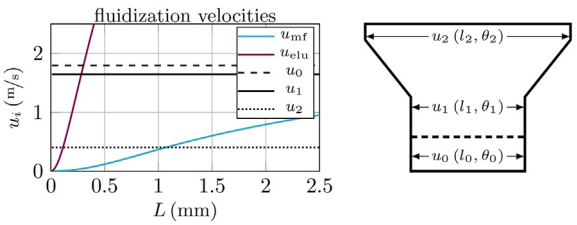

Fig. 3. Left: Velocity of the fluidization medium within the process chamber as well as elutriation u_{elu} and minimum fluidization u_{mf} velocity with respect to particles size **L. Right:** Cross section of the process chamber Procell 25 of Glatt GmbH with corresponding width l_i and temperatures of the fluidization medium θ_i: At bottom $l_0 = 0.25$ m and $\theta_0 = 85$ °C, in the process chamber $l_1 = 0.25$ m and $\theta_1 \approx 50$ °C, and at top $l_2 = 1.0$ m and $\theta_2 \approx 45$ °C.

2. Dynamic model

The following is based on the population balance model (PBM) presented in Dreyschultze et al. [1]. In this model, it is assumed that the granulation chamber is divided into two functional zones. In the first zone, the *spraying zone* (index '1'), the surface of the particles is wetted by the injected solution. In the second zone, the *drying zone* (index '2'), the liquid fraction of the injected solution evaporates from the surface of the particles while the solid fraction remains. Each of the functional zones is considered as well mixed. Particles are assumed to be spherical with diameter L. Agglomeration and breakage are neglected as discussed above.

With these assumptions, the population balance equations of the spraying and the drying zones are

$$\frac{\partial n_1(t,L)}{\partial t} = G\frac{\partial n_1}{\partial L} - \dot{n}_{12} + \dot{n}_{21} + \dot{n}_{1,\text{in}} - \dot{n}_{1,\text{out}} \tag{1}$$

$$\frac{\partial n_2(t,L)}{\partial t} = \dot{n}_{12} - \dot{n}_{21} + \dot{n}_{2,\text{in}} - \dot{n}_{2,\text{out}} \tag{2}$$

Therein, G describes the growth rate, n_i the number density of particles in zone 'i', and $\dot{n}_i$ the particles flows according to Fig. 4:

- $\dot{n}_{12}$ and $\dot{n}_{21}$ describe the particle exchange between the spraying and the drying zone,

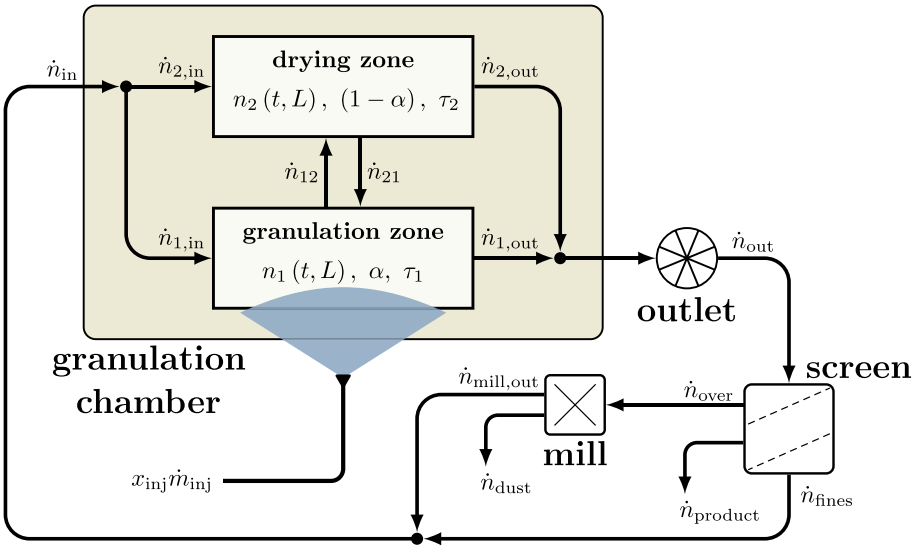

Fig. 4. Flow sheet of the fluidized bed layering granulation with external screen-mill-cycle.

- $\dot{n}_{i,\text{in}}$ the particle inlet to the spraying and the drying zone, and
- $\dot{n}_{i,\text{out}}$ the particle removal from the spraying and the drying zone.

Following Mörl et al. [2], the particle growth rate G is based on a uniform particle growth depending on the total surface of particles in the spraying zone $A_1(t) = \pi\int_0^\infty (L^2 n_1(t,L))dL$, by

$$G = \frac{2x_{\text{inj}}\dot{m}_{\text{inj}}}{\rho_s A_1(t)} \tag{3}$$

with the injection rate $\dot{m}_{\text{inj}}$ and the corresponding mass fraction x_{inj} and mass density ρ_s of the solid fraction within the injected suspension.

The relative volume of particles within the spraying zone

$$\alpha = \frac{\mu_3(n_1)}{\mu_3(n_1)+\mu_3(n_2)} \quad \text{with} \quad \mu_j(n_i) = \int_0^\infty L^j n_i(t,L)dL \tag{4}$$

and the drying zone $(1-\alpha)$ are assumed to be constant.

Thus, the condition $\mu_3(\dot{n}_{12}) = \mu_3(\dot{n}_{21})$ with the particle exchange rates between the spraying and the drying zones

$$\dot{n}_{12}(t,L) = n_1/\tau_1 \quad \text{and} \quad \dot{n}_{21}(t,L) = n_2/\tau_2 \tag{5}$$

are expressed in terms of residence times τ_1 and τ_2. Assuming $\mu_3(\dot{n}_{12}) = \mu_3(\dot{n}_{21})$, yields the following relation between the residence times and α [28]

$$1/\tau_1 = (1-\alpha)/(\alpha\tau_2) \ . \tag{6}$$

Characteristic values for α and τ_2 for different process configurations were given in the literature (see Bück et al. [29] and references therein).

Main differences to the model presented in [1] are related to the calculation of $\dot{n}_{1,\text{in}}, \dot{n}_{1,\text{out}}, \dot{n}_{2,\text{out}}$ in Eqs. (1) and (2), which depend on the product withdrawal, the bed mass control and the model of the mill. These aspects have been modified as follows to gain a better quantitative description of the plant dynamics:

a) The model used in this paper admits a variable total bed mass to simulate the behavior of the bed mass control strategy. In contrast to this, a constant bed mass was assumed in [1] corresponding to an ideal controller.
b) In the experiments to be discussed subsequently, it was observed that larger particles are preferably withdrawn from the bed compared to smaller particles. Therefore, the assumption of a representative product removal from the bed in [1] was replaced by a classified product removal.
c) The model of the mill is crucial for a quantitative prediction of the process dynamics. Therefore, a more detailed model of the mill was identified from stand-alone milling experiments and added to the plant model.

Details of these modifications are given in the following step by step.

2.1. Particle withdrawal from the bed and external product screening

Particles are withdrawn from the process chamber by a rotary valve. It is assumed that the rotary speed of the valve ω_{out} determines the

Table 1
Nomenclature according to the presented fluidized bed layering granulation.

Nomenclature		
A	$(mm^{2)}$	particle surface
d_{32}	(mm)	Sauter mean diameter
e	$(-)$	control error
G	$(^{mm}/_{s})$	growth rate
k	$(-)$	gain
K	$(-)$	gain of the withdrawal
L	(mm)	diameter of particle
L_i	(mm)	separation diameter
$\dot{m}$	$(^{kg}/_{s})$	mass flow rate
n	$(^{1}/_{mm})$	number density of particles
$\dot{n}$	$(^{1}/_{mm})$	number density of particle flow
p	(W)	electrical power
q_0	$(^{1}/_{mm})$	normalized number density of particle
q_3	$(^{1}/_{mm})$	normalized volume density of particle
Q_i	$(^{1}/_{mm})$	cumulative normalized particle size distribution
t	(s)	time
T	$(-)$	separation function
u	$(^{m}/_{s})$	velocity of fluidization medium
x	(s)	mass fraction
Greek letters		
α	$(-)$	relative size of granulation zone
Δp	$(mBar)$	pressure drop
θ	$(°C)$	temperature
$\mu_i(\cdot)$	$(mm^{(i-1)})$	i^{th} order moment of argument
Π_i	$(-)$	parameter set of power of mill
ρ	$(^{kg}/_{mm^3})$	mass density
σ	(mm)	variance of separation
τ	(s)	time constant
ω	$(\%)$	relative rotational velocity

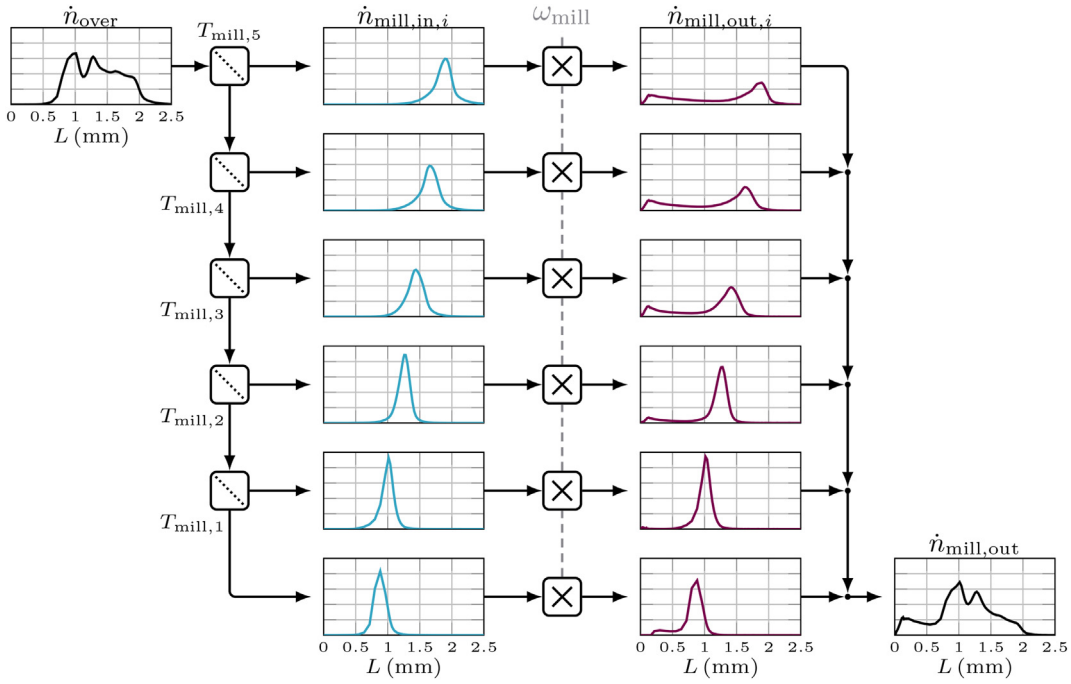

Fig. 5. Scheme of the size-dependent mill model: Oversized particles $\dot{n}_{over}$ are classified into the six fractions $\dot{n}_{mill,in,i}$ by separation functions $T_{mill,i}$. Each fraction i is milled with ω_{mill} to the corresponding $\dot{n}_{mill,out,i}$. Finally, the milled fractions are merged to $\dot{n}_{mill,out}$.

mass flow of the discharged particles by

$$\dot{m}_{out}(t) = k_{out} \cdot \omega_{out} \quad 0 \le \dot{m}_{out} \le \dot{m}_{out,max} \tag{7}$$

Thus, in a first step, ω_{out} is used as manipulated variable to control the bed mass m_{bed}. Bed mass is measured by means of pressure drop across the bed Δp_{bed}, which is in good approximation proportional to the bed mass for constant fluidization conditions applied in the experiments. Control is done with a PI controller according to

$$\omega_{out}(t) = k_{p,out}\left(e_{\Delta p_{bed}} + 1/\tau_{i,out}\int_0^t e_{\Delta p_{bed}}\mathrm{d}t\right) \tag{8}$$

with $0 \le \omega_{out} \le \omega_{out,max}$ and $e_{\Delta p_{bed}}(t) = (\Delta p_{bed,ref} - \Delta p_{bed})$ where $\Delta p_{bed,ref}$ denotes the reference value of the pressure drop.

Based on $\dot{m}_{out}$ the number density flow of the withdrawn particles is calculated with

$$\dot{n}_{out}(t, L) = \dot{n}_{1,out} + \dot{n}_{2,out} \tag{9}$$

$$= KT_{out}(n_1 + n_2) \tag{10}$$

where the drain gain K is determined by

$$K = \frac{\dot{\mu}_{3,out}}{\mu_3(T_{out}(n_1 + n_2))} \tag{11}$$

with $\dot{\mu}_{3,out} = 6\dot{m}_{out}/\pi\rho_s$. The term T_{out} accounts for the classified product removal from the bed which was observed in the experiments. This is modeled with the separation function

$$T_i(L_i, \sigma_i) = \frac{\int_0^L \exp\left(-(L-L_i)^2/(2\sigma_i^2)\right)}{\int_0^\infty \exp\left(-(L-L_i)^2/(2\sigma_i^2)\right)} \tag{12}$$

with separation diameter $L_i = L_{out}$ and variance $\sigma_i = \sigma_{out}$. As will be shown in Section 3, the separation diameter depends on the current particle size distribution of the bed. In particular, it is assumed that L_{out} equals the characteristic value $x_{3,60}$, i.e. the particle size were the cumulative volume based particle size distribution $Q_3(n_1 + n_2)$ equals 0.6:

$$L_{out} = x_{3,60} \quad \text{with} \quad Q_3(L = x_{3,60}) = 0.6\ . \tag{13}$$

Table 2
Parameter set according to the simulation study.

Granulation chamber and injection		
m_{bed}	27.50	(kg)
α	0.05	$(-)$
τ_2	100.00	(s)
x_{inj}	0.35	$(-)$
$\dot{m}_{inj}$	40.00	$(^{kg}/_{h})$
ρ_s	1440.00	$(^{kg}/_{m}^{3})$
Particle withdrawal		
$k_{p,out}$	−60.00	$(^{\%}/_{mm})$
k_{out}	2.00	$(^{kg}/_{\%\cdot h})$
σ_{out}	0.75	(mm)
$\tau_{i,out}$	120.00	(s)
$\omega_{out,max}$	40.00	$(\%)$
Particle screening		
$L_{screen,I}$	1.20	(mm)
$\sigma_{screen,I}$	0.125	(mm)
$L_{screen,II}$	0.80	(mm)
$\sigma_{screen,II}$	0.05	(mm)
Milling process		
k_{bypass}	0.75	$(-)$
$L_{cutsize}$	0.375	(mm)
$\sigma_{cutsize}$	0.105	(mm)
$L_{mill,i}$	[1.01, 1.14, 1.37, 1.58, 1.80]	(mm)
$\sigma_{mill,i}$	[4.05, 13.44, 8.64, 8.58, 9.41]	(mm)
Power of the mill		
$\Pi_{mill,i}$	[−3.09, −286.04, 25.85, 0.04, −0.0008]	$(-)$
τ_{mill}	0.10	$(^{1}/_{s})$
Parameter of controllers		
$k_{p,p_{mill}}$	0.005	$(^{\%}/_{W})$
$\tau_{i,p_{mill}}$	12.00	(s)
$k_{p,d_{32}}$	250.00	$(^{W}/_{mm})$
$p_{mill,0}$	120.00	(W)

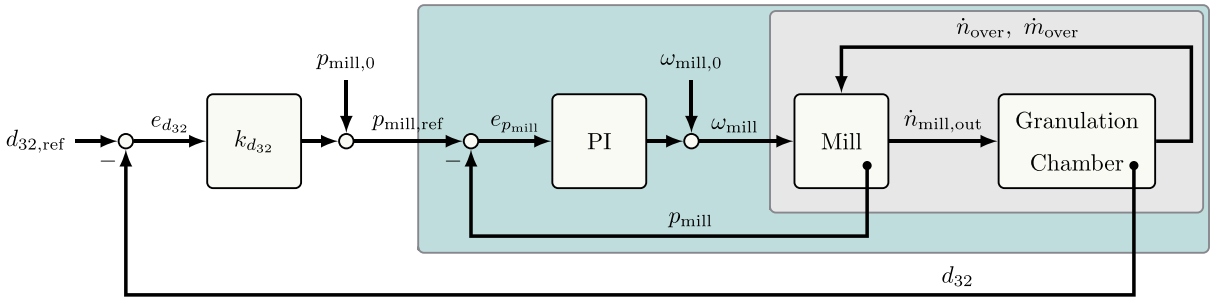

Fig. 6. Control schemes of the experiments: gray configuration was used in experiment 1, green configuration in experiments 2–4, and overall configuration in experiment 5. (For interpretation of the references to colour in this figure legend, the reader is referred to the web version of this article.)

By screening, the withdrawn particles are further classified into three fractions: Fines $\dot{n}_{\text{fines}}$, product $\dot{n}_{\text{product}}$, and oversized $\dot{n}_{\text{over}}$. The screening process is described by

$$\dot{n}_{\text{over}}(t,L) = T_{\text{screen,I}}\ \dot{n}_{\text{out}}\ , \tag{14}$$

$$\dot{n}_{\text{product}}(t,L) = \left(1 - T_{\text{screen,I}}\right) T_{\text{screen,II}}\ \dot{n}_{\text{out}}\ , \text{ and} \tag{15}$$

$$\dot{n}_{\text{fines}}(t,L) = \left(1 - T_{\text{screen,I}}\right)\left(1 - T_{\text{screen,II}}\right)\ \dot{n}_{\text{out}}\ . \tag{16}$$

Again, the separation functions $T_{\text{screen,I}}$ and $T_{\text{screen,II}}$ are given by Eq. (12) with the parameters $\{L_{\text{screen,I}}, \sigma_{\text{screen,I}}\}$ and $\{L_{\text{screen,II}}, \sigma_{\text{screen,II}}\}$ respectively. While the product fraction is removed from the process, the oversized fraction is milled, and together with the fine fraction, recycled to the granulation chamber serving as new nuclei (Table 1).

2.2. Particle milling

The milling of oversized particles has a significant influence on the dynamics of the investigated FBLG process [1,8,12]. Thus, a detailed model of the milling is essential for the quantitative prediction of the plant dynamics. In general, milling of granules is complex. For instance, the type and configuration of the mill as well as particle properties, e.g. porosity and size, have a major influence on the breakage of particles during milling [30,31,32]. Following the ideas in Neugebauer et al. [33], an empirical PBM of the grinding process was established. However, compared to [33] a more detailed model of the mill was developed in the present work taking into account the influence of particle size distribution of the feed to the mill on the grinding processes. Since the PSD of milled particles cannot be measured inline, the following preliminary experimental study was performed: Particles of different sizes were classified into six fractions by screening. Samples of 0.5 kg were milled with the relative rotational velocities $\omega_{\text{mill}} = \{10,15,20,25\}$%, i.e. 24 experiments were performed in total. The PSDs of the samples were determined before and after milling with the CamSizer XT. Based on the measurements, the separation functions of the five screens

$$T_{\text{mill,i}}\left(L_{\text{mill,i}}, \sigma_{\text{mill,i}}\right) = \left(1 + \left(L_{\text{mill,i}}/L\right)^2\right) \exp\left(\frac{\sigma_{\text{mill,i}}}{1 - \left(L/L_{\text{mill,i}}\right)^2}\right) \tag{17}$$

with $i \in \{1,2,3,4,5\}$ were parameterized. Further, the normalized

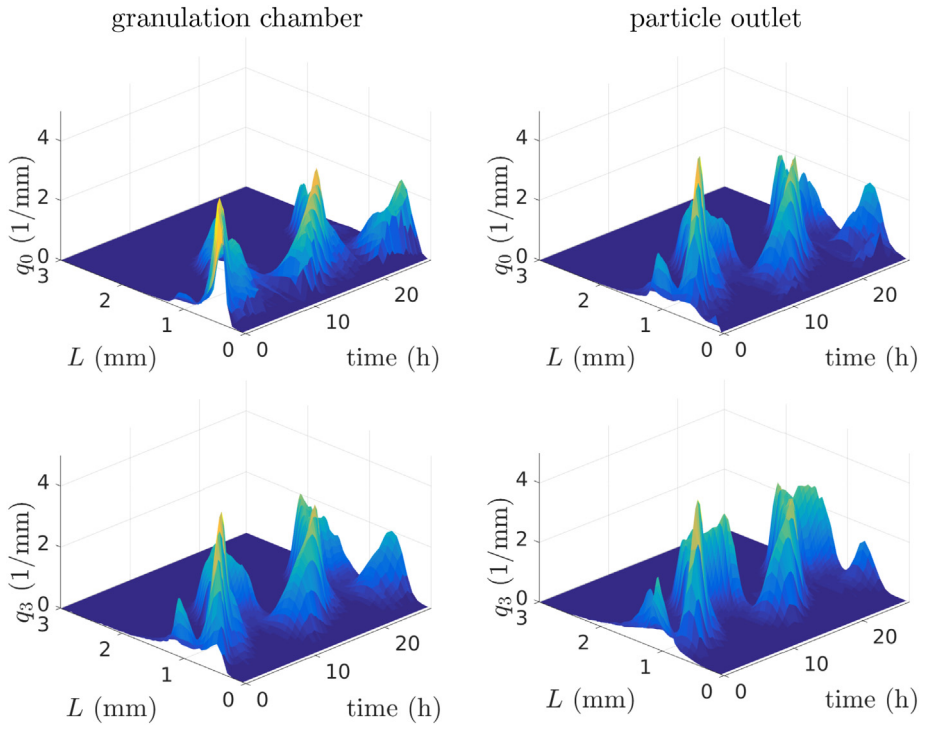

Fig. 7. Experiment 1: Number and volume based, normalized size distributions $q_0(t,L)$ and $q_3(T,L)$ of particles in granulation chamber and particle outlet. The distributions were determined by measuring the taken samples with a CamSizer XT.

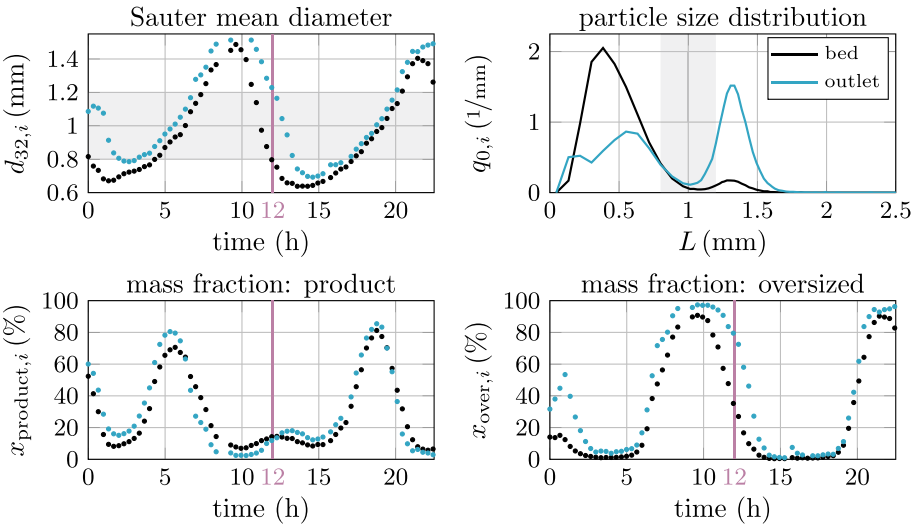

Fig. 8. Experiment 1: **Upper Left:** Sauter mean diameter of particles in granulation chamber and outlet over time. Product range is high-lighted in gray. **Upper Right:** normalized particle size distribution $q_0(t,L)$ of bed and outlet at $t = 12$h. Product range is high-lighted in gray. **Lower left and right:** *mass* fractions of product and oversized particles in bed and outlet.

number densities of the particle size distributions of the milled particle fractions $q_{0,\text{mill,out},i}$ were determined for the different values of ω_{mill}.

These quantities are used for modeling the mill as follows (see also Fig. 5). First $\dot{n}_{\text{over}}$ is separated into six fractions with the according screen functions $T_{\text{mill,i}}$

$$\dot{n}_{\text{mill,in},i}(t,L) = T_{\text{mill},i-1} \prod_{j=i}^{5}(1-T_{\text{mill},j})\dot{n}_{\text{over}} \quad , \quad i \in \{6,5,\ldots,2\} \tag{18}$$

and

$$\dot{n}_{\text{mill,in},1}(t,L) = \prod_{j=1}^{5}(1-T_{\text{mill},j})\dot{n}_{\text{over}} \quad . \tag{19}$$

The relative mass of each fraction i is conserved and determined by $k_{\text{mill},i}(t) = \mu_3(\dot{n}_{\text{mill,in},i})/\mu_3(\dot{n}_{\text{over}})$. Based on $k_{\text{mill},i}$, the milled particle flow rate of each fraction i is determined:

$$\dot{n}_{\text{mill,out},i}(t,L) = k_{\text{mill},i}\frac{q_{0,\text{mill,out},i}(\omega_{\text{mill}},L)}{\mu_3(q_{0,\text{mill,out},i}(\omega_{\text{mill}},L))} \quad . \tag{20}$$

Subsequently, the fractions $\dot{n}_{\text{mill,out},i}$ are merged again. The particle size distribution ω_{mill} of the milled particles were obtained by linear interpolation between available measurements for the specific values of ω_{mill} given above. Further, it is taken into account, that, due to the increased throughput during the continuous FBLG, the efficiency of the milling decreases. For that purpose, a by-pass of particles with gain k_{bypass} is introduced, representing the uncomminuted particles of $\dot{n}_{\text{over}}$:

$$\dot{n}_{\text{mill,out}}(t,L) = k_{\text{bypass}}\dot{n}_{\text{over}} + (1-k_{\text{bypass}})\sum_{i=1}^{6}\dot{n}_{\text{mill,out},i} \quad . \tag{21}$$

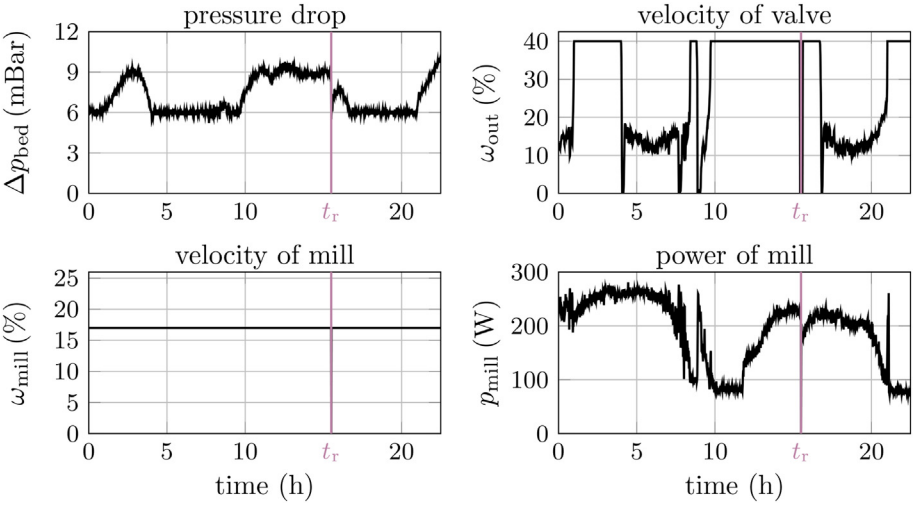

Fig. 9. Experiment 1: measured pressure drop over bed Δp_{bed}, relative rotational speed of the rotary valve at the outlet ω_{out}, relative rotational speed of the mill ω_{mill}, and electrical power of the mill p_{mill}. In the experiment, the mill was operated with a constant $\omega_{\text{mill}} = 17\%$. Alternations of p_{mill} indicate an uneven particle comminution resulting in variations of the Δp_{bed} (reference value: $\Delta p_{\text{bed,ref}} = 6$ mBar). The experiment was interrupted at $t_r = 15.5$ h.

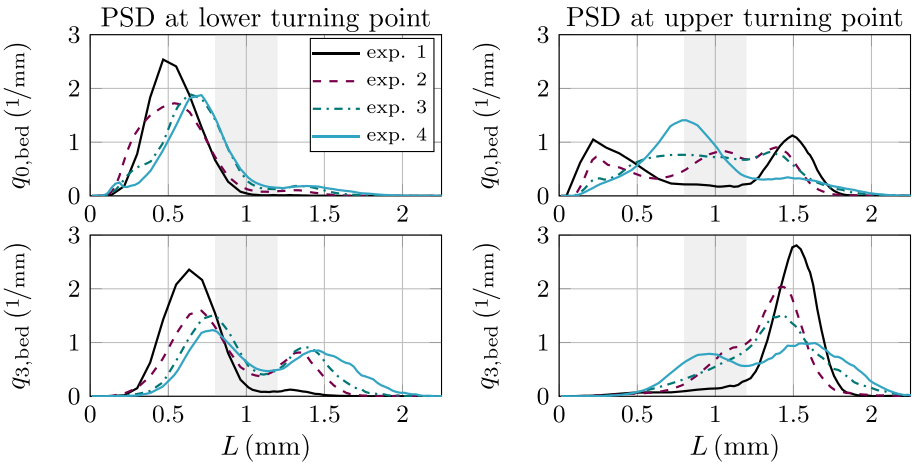

Fig. 10. Particle size distributions of samples at lower and upper turning point of $d_{32,\mathrm{bed}}$ for open-loop experiments 1–4. Corresponding sampling times: experiment 1–13.6 h (lower turning point) and 21.4 h (upper turning point), experiment 2–13.0 h and 10.6 h, experiment 3–33.4 h and 37.7 h, experiment 4–31.3 h and 35.3 h. Product range is highlighted in gray.

Finally, it is assumed, that, because of the fluidization conditions presented in Fig. 3, dust particles are blown out according to

$$\dot{n}_{\mathrm{dust}}(t,L) = (1 - T(L_{\mathrm{cutsize}}, \sigma_{\mathrm{cutsize}}))\dot{n}_{\mathrm{mill,out}} \quad . \tag{22}$$

Again, the separation function $T(L_{\mathrm{cutsize}}, \sigma_{\mathrm{cutsize}})$ is described by Eq. (12). The remaining particles are, together with $\dot{n}_{\mathrm{fines}}$, re-fed to the granulation chamber:

$$\dot{n}_{\mathrm{in}}(t,L) = \dot{n}_{\mathrm{fines}} + T(\mu_{\mathrm{cutsize}}, \sigma_{\mathrm{cutsize}}) \;\; \dot{n}_{\mathrm{mill,out}} \quad . \tag{23}$$

The recycled particles are distributed to the spraying and drying zone with respect to the respective relative volume:

$$\dot{n}_{1,\mathrm{in}}(t,L) = \alpha \;\; \dot{n}_{\mathrm{in}} \quad \text{and} \quad \dot{n}_{2,\mathrm{in}}(t,L) = (1-\alpha)\dot{n}_{\mathrm{in}} \quad . \tag{24}$$

2.3. Numerical solution

The dynamic model was implemented in MATLAB (2018a, MathWorks, Natick, MA, USA, 2018) applying a method of lines approach. Based on a finite volume method approach, the partial differential Eqs. (1) and (2) were discretized using a first order upwind scheme with 200 equidistant grid points in the domain $L = [0,5]$ mm. To solve the resulting system of ordinary equations the MATLAB built-in solver *ode15s* was utilized. The model parameters used for all simulations are shown in Table 2. The initial particle size distributions $n_1(t = 0,L)$ and $n_2(t = 0,L)$ are based on the CamSizer measurement of the first sample of the particle bed of the related experiment.

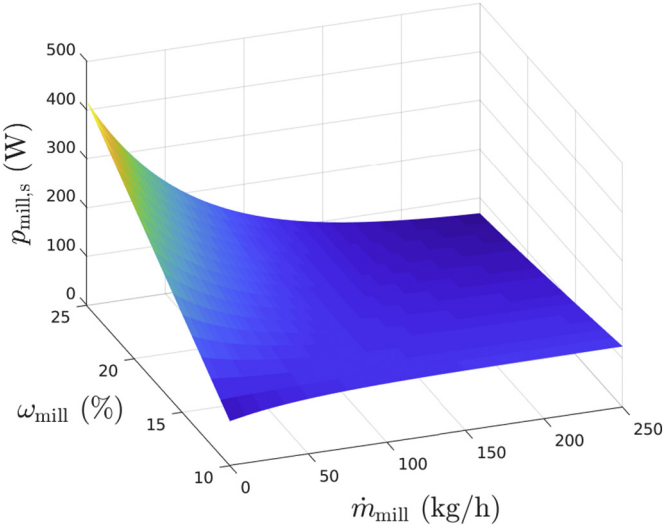

Fig. 11. Black box model of the stationary electrical power of mill: $p_{\mathrm{mill,s}}$ with respect to mill throughput $\dot{m}_{\mathrm{mill}}$ and relative rotational speed of the mill ω_{mill}.

3. Experiments and simulation study

3.1. Operation with constant rotational speed of the mill

In the first experiment, the pin mill was operated with a constant relative rotational speed as introduced in the previous section and illustrated in Fig. 6 with the gray box. This operation mode is the standard configuration of the investigated FBLG and was, for instance, also used by Schmidt et al. [8,9,34].

The corresponding temporal evolution of the number and volume based normalized particle size distribution $q_{0,i}(t,L)$ and $q_{3,i}(t,L)$ of bed and outlet are presented in Fig. 7. The size distributions are characterized by oscillations with long periods. As depicted in Fig. 8, the oscillations can also be observed by monitoring the Sauter mean diameter of bed $d_{32,\mathrm{bed}}$ and outlet $d_{32,\mathrm{out}}$. The Sauter mean diameter, defined as the area-weighted mean size of a particle population and determined by $d_{32,i} = \mu_3(q_{0,i})/\mu_2(q_{0,i})$, is a representative of the PSD. Throughout the experiment, $d_{32,\mathrm{out}}$ was larger than $d_{32,\mathrm{bed}}$. The deviation indicates the classifying impact of the particle withdrawal. As illustrated by the particle size distribution $q_{0,i}$ of bed and outlet, as an example the samples at $t = 12$h are presented in Fig. 8, primarily large particles were discharged from the process chamber.

Because of the oscillations of the PSD, the related mass fractions of fines x_{fines}, product x_{product}, and oversized particles x_{over} varied. As the bed mass is controlled via Δp_{bed} and ω_{out}, see Eqs. (7) and (8), the

Table 3
Overview of the experiments.

ID	Product	ω_{mill}	$p_{\mathrm{mill,ref}}$	$d_{32,\mathrm{ref}}$
1	0.8–1.2 mm	17%	–	–
2	0.8–1.2 mm	–	170 W	–
3	0.8–1.2 mm	–	140 W	–
4	0.8–1.2 mm	–	120 W	–
5	0.8–1.2 mm	–	–	1.2 mm

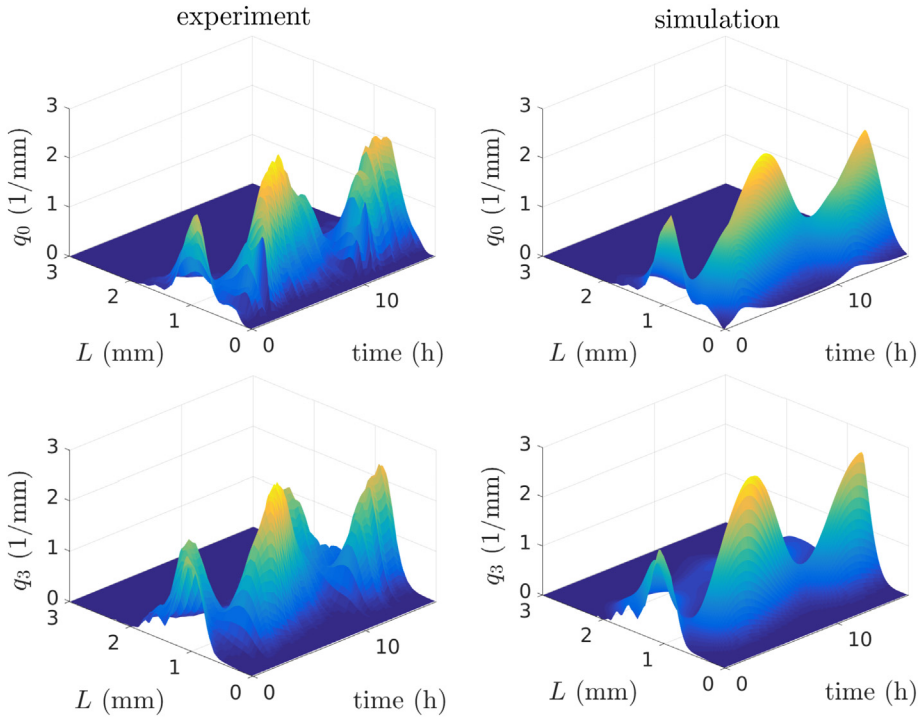

Fig. 12. Left Column: normalized number and volume based particle size distributions $q_{0,\mathrm{bed}}$ and $q_{3,\mathrm{bed}}$ of experiment 2. PSDs were determined with CamSizer XT. **Right Column:** PSDs of the corresponding simulation.

oscillations led to variations of the mass flow of withdrawn particles $\dot{m}_{\mathrm{out}}$. Since $\dot{m}_{\mathrm{out}}$ cannot be measured online, the variations of $\dot{m}_{\mathrm{out}}$ can only be observed by monitoring the rotational speed of the rotary valve at the particle outlet ω_{out}. As shown in Fig. 9, ω_{out} varied in the range of $[0,\omega_{\mathrm{out,max}}]$ throughout the experiment. Based on previous experiments, the upper limit $\omega_{\mathrm{out,max}}$ was found to be 40% as a further increase of ω_{out} did not raise $\dot{m}_{\mathrm{out}}$. It is due to this restriction that not enough product particles were discharged from the FBLG. This was exacerbated by the classifying particle withdrawal: in the outlet, product particles were displaced by oversized particles (see Fig. 8). The insufficient product removal induced a rise of m_{bed} and, as illustrated in Fig. 9, an increase of the pressure drop Δp_{bed}. Similar patterns of behavior were observed by Schmidt [34]. In the present case, the continuously increasing bed mass finally led to the shutdown of the process.

In addition, the classifying outlet induced an overgrowing of particles in the further course of the experiment. Particles of product fraction were not withdrawn from the process chamber in a sufficient quantity. In consequence, particle growth proceeded such that the particles entered the oversized fraction. This is illustrated in Fig. 10. There, $q_{0,\mathrm{bed}}$ and $q_{3,\mathrm{bed}}$ at a local minimum and maximum, in the following denoted as turning points, of $d_{32,\mathrm{bed}}$ are shown for the experiments 1–4. Of special interest are the modes, viz. the peaks, of the PSDs. At the lower turning point, $t = 13.6$ h, the modes of the PSDs are in the fines fractions. In the progress of the experiment, the particles have grown, leading to a shift of the modes to higher particles sizes. At $t = 21.4$ h, the upper turning point of $d_{32,\mathrm{bed}}$, the modes are in the oversized fraction. In consequence, the mass portion x_{over} in bed and outlet increased resulting in a higher mill throughput $\dot{m}_{\mathrm{mill}}$.

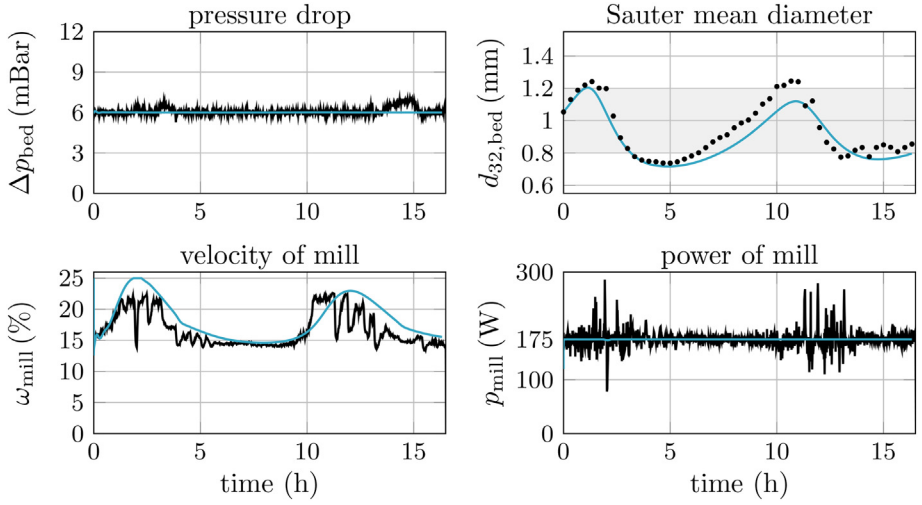

Fig. 13. Comparison of selected data of experiment 2 (black line) and the corresponding simulation results (blue line). By adjusting ω_{mill}, the mill was operated with constant $p_{\mathrm{mill}} = 175$ W. While Δp_{bed} is at a constant level, the Sauter mean diameter $d_{32,\mathrm{bed}}$ is characterized by non-linear oscillations. The measured Sauter mean diameter is based on the measurements of the CamSizer XT. (For interpretation of the references to colour in this figure legend, the reader is referred to the web version of this article.)

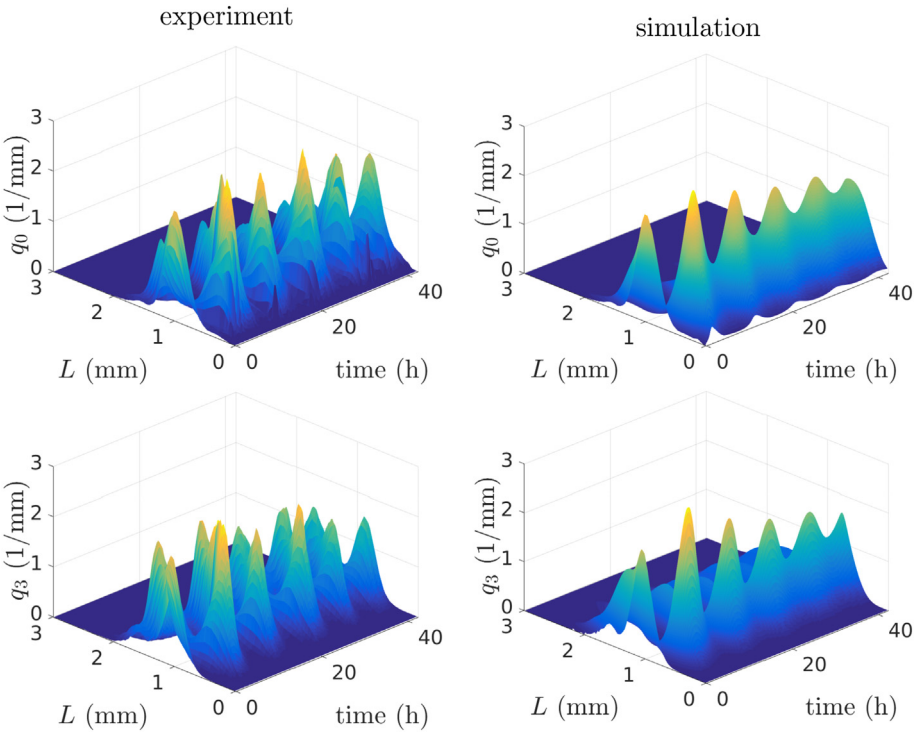

Fig. 14. Left Column: normalized number and volume based particle size distributions $q_{0,bed}$and $q_{3,bed}$ of experiment 3. PSDs were determined with CamSizer XT. **Right Column:** PSDs of the corresponding simulation.

As illustrated in Fig. 9, the milling process is influenced by $\dot{m}_{mill}$. An increase of the mill throughput, characterized by high values of ω_{out} and x_{over}, led to a decrease of the electrical power consumption of the mill p_{mill}. This indicates, in combination with the large maxima of $d_{32,bed}$ and $d_{32,out}$, the inadequate comminution of oversized particles. The uneven milling supported the overgrowing of the particles and therefore the occurrence of the observed oscillations.

3.2. Closed loop control of the mill power

To enable an even milling of oversized particles feedback control was applied to keep the mill power constant at a given reference value by readjusting the rotational speed of the mill. For this purpose again a PI controller was used. The block diagram of the control loop is illustrated in green in Fig. 6. The dynamic model was extended accordingly. In particular, it was assumed, that the dynamic behavior of p_{mill} can be described by a first order lag element (PT_1):

$$\dot{p}_{mill}(t) = (p_{mill,s} - p_{mill})/\tau_{mill} \tag{25}$$

As indicated by experimental findings, the stationary value of the electrical power $p_{mill,s}$ depends on ω_{mill} and the mass throughput $\dot{m}_{mill} = (\pi\rho_s/6)\mu_3(\dot{n}_{over})$. Based on previous measurements, the correlation

$$p_{mill,s}(\omega_{mill}, \dot{m}_{mill}) = \Pi_1 + \Pi_2\omega_{mill} + (\Pi_3 + \Pi_4\omega_{mill})\exp(-(\Pi_5 + \Pi_6\omega_{mill})\dot{m}_{mill}) \tag{26}$$

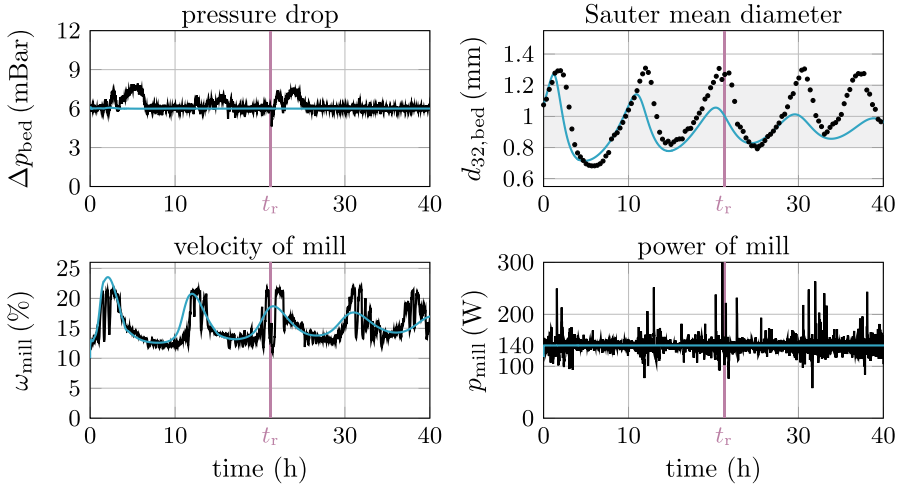

Fig. 15. Comparison of selected data of experiment 3 (black line) and the corresponding simulation (blue line). The mill was operated with constant $p_{mill} = 140$W. While Δp_{bed} is at a constant level, the Sauter mean diameter $d_{32,bed}$ is characterized by slow decaying, non-linear oscillations. The measured Sauter mean diameter is based on the measurements of the CamSizer XT, the experiment was interrupted at $t_r = 21.25$ h. (For interpretation of the references to colour in this figure legend, the reader is referred to the web version of this article.)

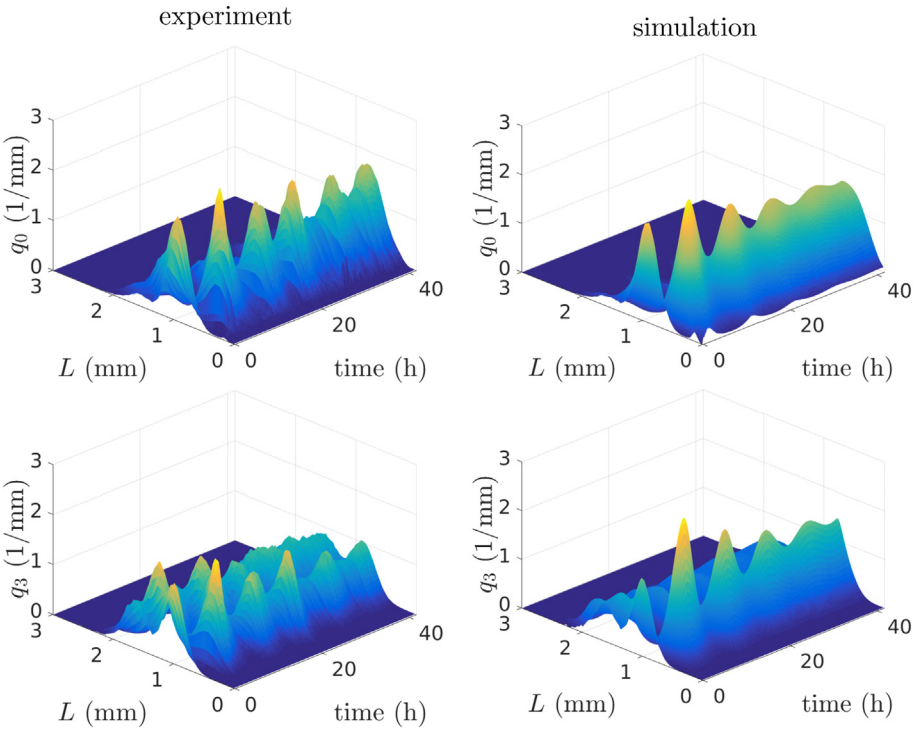

Fig. 16. Left Column: normalized number and volume based particle size distributions $q_{0,\mathrm{bed}}$ and $q_{3,\mathrm{bed}}$ of experiment 4. PSDs were determined with CamSizer XT. **Right Column:** PSDs of the corresponding simulation.

was established by a least square fit. The functional correlation of $p_{\mathrm{mill,s}}$ and its arguments is presented in Fig. 11.

To study the influence of the milling on the process stability, experiments 2–4 were performed with different reference values of the mill power $p_{\mathrm{mill,ref}}$. The set-points of the different experiments are presented in Table 3. Following Dreyschultze et al. [1] and Radichkow et al. [12], it is expected that a reduction of $p_{\mathrm{mill,ref}}$ leads to an enhanced process stability. Throughout the experiments 2–4, the classifying effect of the particle withdrawal described in the previous section is observed again.

In experiment 2, the mill was operated with $p_{\mathrm{mill,ref}} = 175$ W. The results are presented in Figs. 12 and 13. Again, $q_{0,\mathrm{bed}}$ and $q_{3,\mathrm{bed}}$ are characterized by oscillations. As shown in Fig. 10 the measured PSDs are now more compact than in the first experiment: Firstly, the distance between the modes of $q_{0,\mathrm{bed}}$ and $q_{3,\mathrm{bed}}$ at lower ($t = 13.0$ h) and upper turning point of $d_{32,\mathrm{bed}}$ ($t = 10.6$ h) narrowed. Secondly, the amplitudes of the corresponding modes decreased. This leads, as depicted in Fig. 13, to a decrease in the amplitudes of $d_{32,\mathrm{bed}}$. In consequence, the mass portion of the product fraction is of sufficient size throughout the experiment. Thus, the adequate removal of product particles from the FBLG is guaranteed such that, as monitored by the pressure drop Δp_{bed}, the bed mass m_{bed} is constant over time. Although the operating conditions of the FBLG are constant, the intense milling of oversized particles induced the formation of a large number of small nuclei. In accordance with [1], this leads to the formation of self-sustained oscillation of the PSDs. Therefore, it was not expected that the process settles down to a stable steady state so that the experiment was terminated at $t = 17$ h.

In experiment 3, the reference value of the electrical power of the mill $p_{\mathrm{mill,ref}}$ was reduced to 140 W. Due to the large run-time of 40 h,

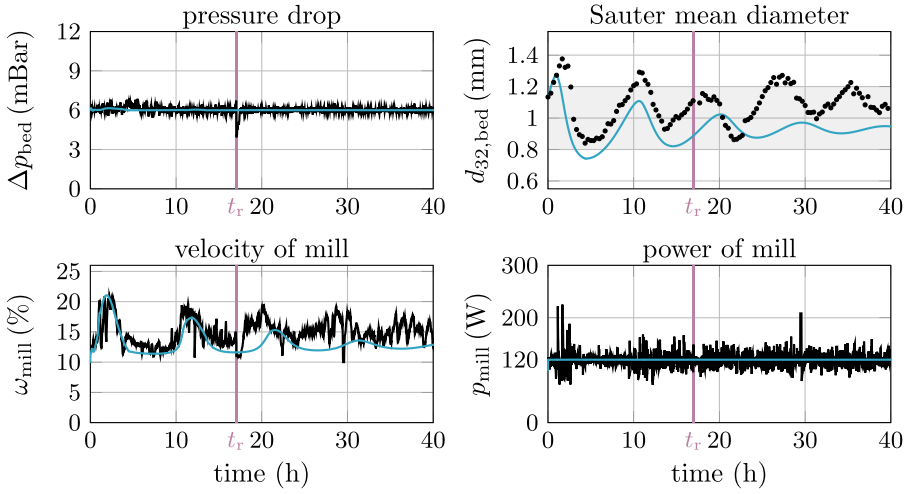

Fig. 17. Comparison of selected data of experiment 4 (black line) and the corresponding simulation results (blue line). The mill was operated with constant $p_{\mathrm{mill}} = 120$ W. While Δp_{bed} is at a constant level, the Sauter mean diameter $d_{32,\mathrm{bed}}$ is characterized by decaying, non-linear oscillations. The measured Sauter mean diameter is based on the measurements of the CamSizer XT, the experiment was interrupted at $t_r = 17.0$ h. (For interpretation of the references to colour in this figure legend, the reader is referred to the web version of this article.)

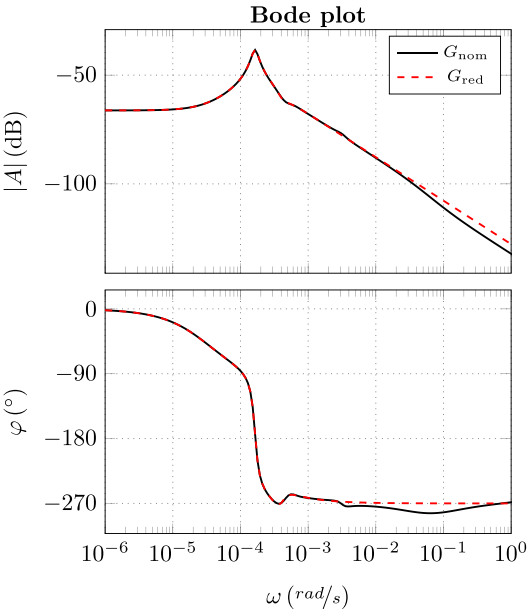

Fig. 18. Bode plots of the full order system $G_{nom}(j\omega)$ and the reduced system $G_{red}(j\omega)$ of order 5.

the experiment was interrupted after 21.25 h of process time and restarted again. Figs. 14 and 15 present the related particle size distributions of the bed and further measurement information. Once again, Δp_{bed} and p_{mill} are at a constant level throughout the experiment. Due to the decreased p_{mill}, the particle grinding was reduced. As shown in Fig. 10, the modes of $q_{0,bed}$ and $q_{3,bed}$ shifted to a larger particle size L at the lower turning point of $d_{32,bed}$ at $t = 33.4$ h. This leads to a more even particle growth resulting in a slow decay of the oscillations of the particle size distributions and, in consequence, of the oscillations of $d_{32,bed}$.

Afterwards, $p_{mill,ref}$ was further reduced to 120 W in experiment 4. Related PSDs and measurements are presented in Figs. 16 and 17. In experiment 4, a faster decay of the oscillatory behavior is observed compared to experiment 3. As illustrated in Fig. 10, the deviations between the PSDs at the lower and upper turning point of $d_{32,bed}$, sampling times are $t = 31.3$ h and $t = 35.3$ h, are, compared to the previous experiments 1–3, quite small. It is expected, that in the further course of the process these deviations would vanish such that the process would reach stable steady-state conditions. However, the decay to steady state is very slow due to the oscillatory behavior. In addition, the settling is aggravated by disturbances, such as the restart of the FBLG at $t_r = 17$ h. Therefore, the experiment was terminated at $t = 40$ h.

Comparison between experiments and model predictions are also shown in Figs. 12–17 for experiments 2–4. In general, simulation results and experimental findings are in good agreement. The maximum values of $q_{0,bed}$ and $q_{3,bed}$, as well as the period of the oscillations in Figs. 12, 14, and 16, are at the same level resulting in a similar shape of measured and simulated PSDs. Furthermore, Figs. 13, 15, and 17 show the good agreement of p_{mill} and ω_{mill} between experiments and simulations. With respect to $p_{mill,ref}$, the model is capable to reproduce the different forms of dynamic behavior. As illustrated in Fig. 12, $p_{mill,ref} = 170$ W induced oscillations of $q_{0,bed}$ and $q_{3,bed}$ with large amplitudes. In contrast to this, the PSDs are characterized by slowly decaying oscillations for $p_{mill,ref} = 140$ W and $p_{mill,ref} = 120$ W (see Figs. 14 and 16).

3.3. Additional closed loop control of the Sauter mean diameter

To enhance the dynamics of the process and establish operation with constant PSD as fast as possible, a cascade controller was designed: As illustrated in Fig. 6, the PI-controller for the bed mass is extended by an outer loop to control the Sauter mean diameter $d_{32,bed}$ by readjusting the reference value of the mill power $p_{mill,ref}$. The plant model presented in this paper was used for controller design. As a first step, the dynamic model is numerically linearized at the stationary state according to the default parameter set with $p_{mill,ref} = 120$ W. The resulting linear time-invariant (LTI) transfer function $G_{nom}(j\omega)$ of order 403 describes the dynamic behavior of the output signal $d_{32,bed}$ with respect to the input signal $p_{mill,ref}$ in the neighborhood of the steady state. By means of a balanced truncation, the full-order system is reduced to a system of order 5 [35]. The reduced model $G_{red}(j\omega)$ shows good agreement with the nominal system $G_{nom}(j\omega)$ as illustrated with the Bode plots in Fig. 18.

Based on the transfer function $G_{red}(j\omega)$, a feedback controller is designed by means of the root locus method [36]. Root loci represent the location of the closed loop poles in the complex plane depending on the controller gain. They are illustrated in Fig. 19 for a P controller (left figure) compared to a PI controller (right figure). They start in

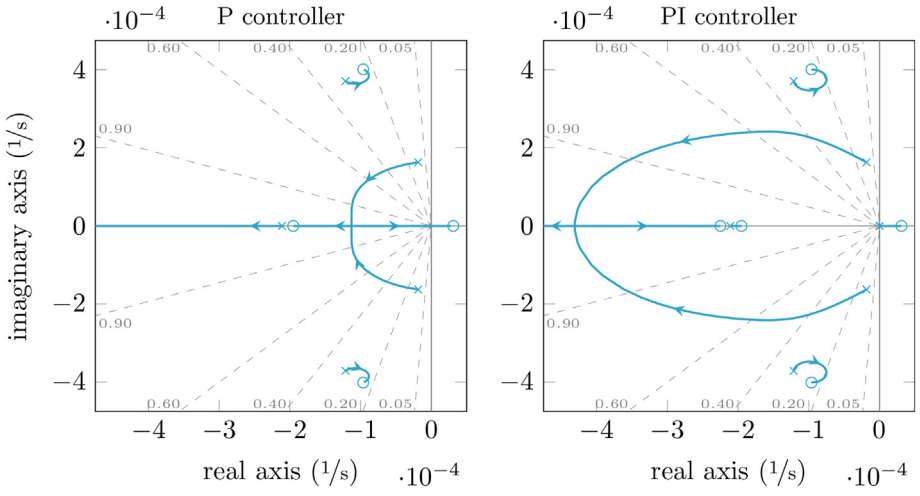

Fig. 19. The root-locus of the closed-loop system $G_{cl}(j\omega)$with respect to controller gain $k_{d_{32}}$. Poles of $G_{ol}(j\omega)$ are indicated by x, the according zero by o. The damping ratios of $G_{cl}(j\omega)$ are specified in gray. Left: A suitable tuned P controller $k_{d_{32}}$ increases the damping ratio of $G_{cl}(j\omega)$ and guarantees a stable steady-state operation. Right: Due to the pole introduced at the origin, one pole of the PI controlled closed-loop system is in the right half-plane hence $G_{cl}(j\omega)$ is unstable for all $k_{d_{32}}$.

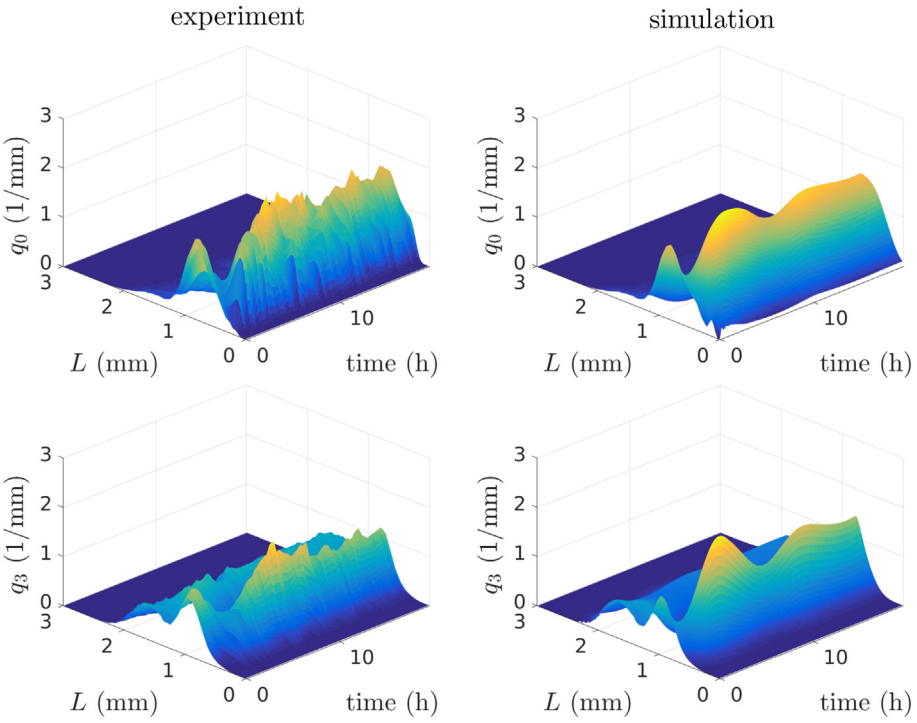

Fig. 20. Left Column: normalized number and volume based particle size distributions $q_{0,\mathrm{bed}}$ and $q_{3,\mathrm{bed}}$ of experiment 5. PSDs were determined with CamSizer XT. **Right Column:** PSDs of the corresponding simulation.

the open loop poles of the controller and the system to be controlled indicated by the crosses in Fig. 19 and end in the open loop zeros indicated by the circles in Fig. 19. In both diagrams one branch is tending to $-\infty$. The controlled LTI system is stable if and only if all closed loop poles lie in the left half plane. Usually, controllers with integral action are preferred in view of steady state accuracy [36]. However, from Fig. 19 it is readily concluded, that the system is not stabilizable if the controller includes integral action like the PI controller in the right diagram. This is due to the fact, that any integral action introduces an open loop pole in the origin and that the branch starting from the origin lies entirely in the right half plane. Therefore, a P controller was selected, which allows stabilization with good damping for some suitable controller gain as illustrated in the left diagram. From this diagram, we further conclude that this will even work for higher mill powers when the open loop system becomes unstable and the pair of conjugate complex poles of the plant close to the imaginary axis is shifted from the left to the right half plane.

In the next step, the designed P controller was validated with a simulation study. For this purpose, the nonlinear dynamic plant model presented in Section 2 was extended by the controller according to

$$p_{\mathrm{mill,ref}}(t) = k_{d_{32}} e_{d_{32,\mathrm{bed}}} + p_{\mathrm{mill},0} \tag{27}$$

with the control error $e_{d_{32,\mathrm{bed}}} = d_{32,\mathrm{ref}} - d_{32,\mathrm{bed}}$.

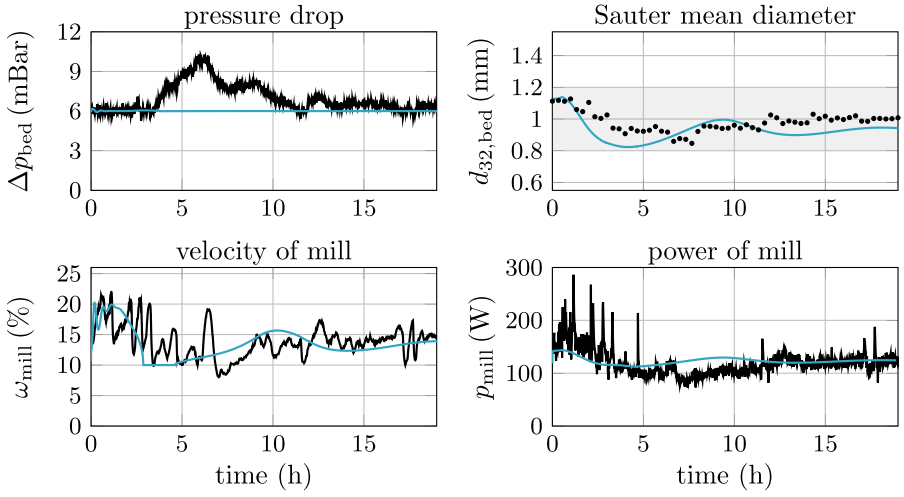

Fig. 21. Comparison of selected data of experiment 5 (black line) and the corresponding simulation results (blue line). Based on the inline measured particles size distribution the process is controlled. The related control scheme is presented in Fig. 6. After a sufficient time the process settles at steady state characterized by constant Δp_{bed} and $d_{32,\mathrm{bed}}$. (For interpretation of the references to colour in this figure legend, the reader is referred to the web version of this article.)

As the simulation results were promising, the designed P controller was implemented at the plant and tested in experiment 5. The Sauter mean diameter was measured inline with the equipped Parsum probe.

Simulation and experimental results are illustrated in Figs. 20 and 21. It is shown that the overall control strategy dampens the oscillations of $d_{32,\mathrm{bed}}$ and thus also the oscillations of the PSD within relatively short time and achieves a stable steady state with constant bed mass m_{bed}. Compared to the corresponding scenario without control of the Sauter mean diameter which was shown in Fig. 17, the process dynamics were improved significantly. In Fig. 17 a stable steady state could not be achieved within the first 40 hours, whereas in Figs. 20 and 21 a stable steady state is reached within 5 hours. Again, there is a good agreement between simulation and experiments.

4. Conclusion

In this article, control strategies for stabilizing the bed mass and the particle size distribution of a continuous fluidized bed layering granulation process with sieve-mill-cycle were developed step by step and validated experimentally. For the first time, it was shown experimentally, that the process dynamics can be improved considerably by using even relatively simple control strategies. The theoretical development was based on an extended plant model, accounting for a more realistic description of the product removal, the grinding of the oversized particles and the bed mass control compared to our previous work [1,12,33]. The model showed good agreement with the experimental findings and can be used for further studies on dynamics and control of continuous FBLG processes.

Future work will focus on a rigorous evaluation of more advanced control strategies as described for example in [16,23]. Furthermore, the dynamic model can be extended to account for other important particle properties, like particle porosity, for example [37]. Such a model could be used to develop and test more advanced process configurations in silico. A typical example are multi chamber processes, which admit different operating conditions in different process chambers and can therefore be used for the formulation of more advanced particles. To enhance the performance of those processes and guarantee the formation of particles with desired properties, suitable control strategies for multi chamber processes can also be developed using such an extended dynamic model.

Acknowledgments

The financial support of DFG (Deutsche Forschungsgemeinschaft) within the priority program SPP 1679 is gratefully acknowledged.

References

[1] C. Dreyschultze, C. Neugebauer, S. Palis, A. Bück, E. Tsotsas, S. Heinrich, A. Kienle, Influence of zone formation on stability of continuous fluidized bed layering granulation with external product classification, Particuology 23 (2015) 1–7.
[2] L. Mörl, S. Heinrich, M. Peglow, Fluidized bed spray granulation, in: M.H.A.D. Salman, J. Seville (Eds.), Granulation, Vol. 11 of Handbook of Powder Technology, Elsevier Science B.V 2007, pp. 21–188.
[3] E. Tsotsas, Influence of drying kinetics on particle formation: A personal perspective, Dry. Technol. 30 (11−12) (2012) 1167–1175.
[4] G. Grünewald, B. Westhoff, M. Kind, Fluidized bed spray granulation: Nucleation studies with steady-state experiments, Dry. Technol. 28 (3) (2010) 349–360.
[5] I. Cotabarren, P.G. Schulz, V. Bucalá, J. Piña, Modeling of an industrial double-roll crusher of a urea granulation circuit, Powder Technol. 183 (2) (2008) 224–230.
[6] R. Schütte, A. Ruhs, I. Pelgrim, C.-J. Klasen, L. Kaiser, Fluidised Bed Spray Granulation Process Producing Two or more Different Size Distributions, 1998.
[7] M. Schmidt, A. Bück, E. Tsotsas, Experimental investigation of process stability of continuous spray fluidized bed layering with internal separation, Chem. Eng. Sci. 126 (2015) 55–66.
[8] M. Schmidt, C. Rieck, A. Bück, E. Tsotsas, Experimental investigation of process stability of continuous spray fluidized bed layering with external product separation, Chem. Eng. Sci. 137 (2015) 466–475.
[9] M. Schmidt, A. Bück, E. Tsotsas, Experimental investigation of the influence of drying conditions on process stability of continuous spray fluidized bed layering granulation with external product separation, Powder Technol. 320 (2017) 474–482 Supplement C.
[10] A. Vreman, C. van Lare, M. Hounslow, A basic population balance model for fluid bed spray granulation, Chem. Eng. Sci. 64 (21) (2009) 4389–4398 390.
[11] C. Neugebauer, S. Palis, A. Bück, E. Tsotsas, S. Heinrich, A. Kienle, A dynamic two-zone model of continuous fluidized bed layering granulation with internal product classification, Particuology 31 (2017) 8–14.
[12] R. Radichkov, T. Müller, A. Kienle, S. Heinrich, M. Peglow, L. Mörl, A numerical bifurcation analysis of continuous fluidized bed spray granulation with external product classification, Chem. Eng. Process. Process Intensif. 45 (10) (2006) 826–837.
[13] T. Hoffmann, C. Rieck, M. Schmidt, A. Bück, M. Peglow, E. Tsotsas, Prediction of shell porosities in continuous fluidized bed spray layering, Dry. Technol. 33 (13) (2015) 1662–1670.
[14] C. Rieck, T. Hoffmann, A. Bück, M. Peglow, E. Tsotsas, Influence of drying conditions on layer porosity in fluidized bed spray granulation, Powder Technol. 272 (2015) 120–131.
[15] E. Diez, K. Meyer, A. Bück, E. Tsotsas, S. Heinrich, Influence of process conditions on the product properties in a continuous fluidized bed spray granulation process, Chem. Eng. Res. Des. 139 (2018) 104–115.
[16] S. Palis, A. Kienle, Stabilization of continuous fluidized bed spray granulation with external product classification, Chem. Eng. Sci. 70 (2012) 200–209 4th International Conference on Population Balance Modeling.
[17] S. Palis, A. Kienle, H_∞ loop shaping control for continuous fluidized bed spray granulation with internal product classification, Ind. Eng. Chem. Res. 52 (1) (2013) 408–420.
[18] S. Palis, C. Dreyschultze, C. Neugebauer, A. Kienle, Auto-tuning control systems for improved operation of continuous fluidized bed spray granulation processes with external product classification, Proc. Eng. 102 (2015) 133–141 new Paradigm of Particle Science and Technology Proceedings of The 7th World Congress on Particle Technology.
[19] S. Palis, Non-identifier-based adaptive control of continuous fluidized bed spray granulation, J. Process Control 71 (2018) 46–51.
[20] A. Bück, S. Palis, E. Tsotsas, et al., Powder Technology 270 (Part B) (2015) 575–583 (6th International Workshop on Granulation: Granulation across the length scales).
[21] A. Bück, R. Dürr, M. Schmidt, E. Tsotsas, Model predictive control of continuous layering granulation in fluidis ed beds with internal product classification, J. Process Control 45 (2016) 65–75.
[22] S. Palis, A. Kienle, Discrepancy based control of continuous fluidized bed spray granulation with internal product classification, IFAC Proc. Vol. 45 (15) (2012) 756–761 8th IFAC Symposium on Advanced Control of Chemical Processes.
[23] S. Palis, A. Kienle, Discrepancy based control of particulate processes, J. Process Control 24 (3) (2014) 33–46.
[24] I.M. Cotabarren, D.E. Bertn, V. Bucal, J. Pia, Feedback control strategies for a continuous industrial fluidized-bed granulation process, Powder Technol. 283 (2015) 415–432.
[25] S. Palis, C. Neugebauer, A. Bück, S. Heinrich, E. Tsotsas, A. Kienle, Control of multi-chamber continuous fluidized bed spray granulation, Proceedings of PARTEC 2016 2016, pp. 1–4.
[26] B.J. Ennis, G. Tardos, R. Pfeffer, A microlevel-based characterization of granulation phenomena, Powder Technol. 65 (1) (1991) 257–272 a Special Volume Devoted to the Second Symposium on Advances in Particulate Technology.
[27] D. Petrak, Simultaneous measurement of particle size and particle velocity by the spatial filtering technique, Part. Part. Syst. Charact. 19 (6) (2002) 391–400.
[28] N. Hampel, A. Bück, M. Peglow, E. Tsotsas, Continuous pellet coating in a wurster fluidized bed process, Chem. Eng. Sci. 86 (0) (2013) (450 87 – 98, 5th International Granulation Workshop).
[29] A. Bück, C. Neugebauer, K. Meyer, S. Palis, E. Diez, A. Kienle, S. Heinrich, E. Tsotsas, Influence of operation parameters on process stability in continuous fluidised bed layering with external product classification, Powder Technol. 300 (2016) 37–45.
[30] S. Antonyuk, J. Tomas, S. Heinrich, L. Mörl, Breakage behaviour of spherical granulates by compression, Chem. Eng. Sci. 60 (14) (2005) 4031–4044.
[31] S. Antonyuk, M. Khanal, J. Tomas, S. Heinrich, L. Mörl, Impact breakage of spherical granules: experimental study and dem simulation, Chem. Eng. Process. Process Intensif. 45 (10) (2006) 838–856 (particulate Processes A Special Issue of Chemical Engineering and Processing).
[32] L. Vogel, W. Peukert, Breakage behaviour of different materials-construction of a mastercurve for the breakage probability, Powder Technol. 129 (1) (2003) 101–110.
[33] C. Neugebauer, S. Palis, A. Bück, E. Diez, S. Heinrich, E. Tsotsas, A. Kienle, Influence of mill characteristics on stability of continuous layering granulation with external product classification, in: Z. Kravanja, M. Bogataj (Eds.), 26th European Symposium on Computer Aided Process Engineering, Vol. 38 of Computer Aided Chemical Engineering, Elsevier 2016, pp. 1275–1280.
[34] M. Schmidt, Process Dynamics and Structure Formation in Continuous Spary Fluidized Bed Processes, Ph.D. thesis Otto-von-Guericke-Universität, April 2018.
[35] S. Skogestad, I. Postlethwaite, Multivariable Feedback Control: Analysis and Design, 2nd edition John Wiley & Sons Ltd, 2007.
[36] R.C. Dorf, R.H. Bishop, Modern Control Systems, 13th edition Pearson, 2017.
[37] C. Neugebauer, A. Bück, S. Palis, L. Mielke, E. Tsotsas, A. Kienle, Influence of thermal conditions on particle properties in fluidized bed layering granulation, Processes 6 (12) (2019).